

Monotone, Bi-Lipschitz, and Polyak-Łojasiewicz Networks

Ruigang Wang
 The University of Sydney
 ruigang.wang@sydney.edu

Krishnamurthy (Dj) Dvijotham
 Google DeepMind
 dvij@google.com

Ian R. Manchester
 The University of Sydney
 ian.manchester@sydney.edu.au

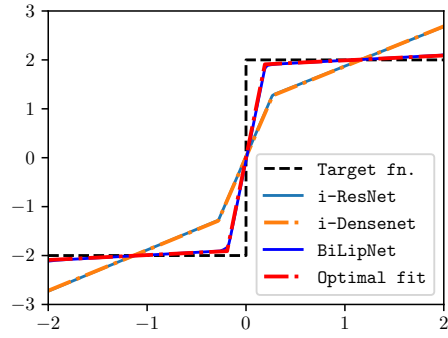
Abstract

This paper presents a new *bi-Lipschitz* invertible neural network, the BiLipNet, which has the ability to control both its *Lipschitzness* (output sensitivity to input perturbations) and *inverse Lipschitzness* (input distinguishability from different outputs). The main contribution is a novel invertible residual layer with certified strong monotonicity and Lipschitzness, which we compose with orthogonal layers to build bi-Lipschitz networks. The certification is based on incremental quadratic constraints, which achieves much tighter bounds compared to spectral normalization. Moreover, we formulate the model inverse calculation as a three-operator splitting problem, for which fast algorithms are known. Based on the proposed bi-Lipschitz network, we introduce a new scalar-output network, the PLNet, which satisfies the Polyak-Łojasiewicz condition. It can be applied to learn non-convex surrogate losses with favourable properties, e.g., a unique and efficiently-computable global minimum.

1 Introduction

In many applications, it is desirable to learn neural networks with *guaranteed input-output behaviors*, i.e., certain properties that are ensured by design. For example, Lipschitz-bounded networks have proven to be beneficial to stabilization of generative adversarial network (GAN) training Arjovsky et al. (2017); Gulrajani et al. (2017), certifiable robustness against adversarial attacks Tsuzuku et al. (2018); Revay et al. (2020); Singla and Feizi (2021); Pauli et al. (2021); Prach and Lampert (2022); Araujo et al. (2023); Wang and Manchester (2023) and robust reinforcement learning Russo and Proutiere (2021).

Another input-output property – *invertibility* has re-



Model	inv. Lip.	Lip.	loss
i-ResNet	0.80	4.69	0.2090
i-DenseNet	0.82	4.66	0.2091
BiLipNet	0.11	9.97	0.0685
Optimal	0.10	10.0	0.0677

Figure 1: Fitting a step function, which is not Lipschitz, with certified $(0.1, 10)$ -Lipschitz models. Compared to the analytically-computed optimum, the proposed BiLipNet achieves much tighter bounds than models based on spectral normalization.

ceived much attention in the deep learning literature since the introduction of *normalizing flows* Dinh et al. (2015) for probability-density learning. Invertible neural networks (INNs) have been applied in applications such as generative modeling Dinh et al. (2017); Kingma and Dhariwal (2018), probabilistic inference Bauer and Mnih (2019); Ward et al. (2019); Louizos and Welling (2017), solving inverse problems Ardizzone et al. (2018) and uncertainty estimation Liu et al. (2020). A common way to construct INNs is to compose simple invertible transformations and sophisticated invertible layers, including coupling flows Dinh et al. (2017); Kingma and Dhariwal (2018), auto-regressive models Huang et al. (2018); De Cao et al. (2020); Ho et al. (2019), invertible residual layers Chen et al. (2019); Behrmann

et al. (2019), monotone networks Ahn et al. (2022), and neural ordinary differential equations Grathwohl et al. (2019), see also in the surveys Papamakarios et al. (2021); Kobyzev et al. (2020).

However, Behrmann et al. (2021) observed that commonly-used INNs suffer from exploding inverses and are thus prone to becoming numerically non-invertible. This observation motivates the input-output property of *bi-Lipschitzness*. A layer $\mathcal{F} : \mathbb{R}^n \rightarrow \mathbb{R}^n$ is said to be bi-Lipschitz with bound of (μ, ν) , or simply (μ, ν) -Lipschitz, if the following inequalities hold for all $x, x' \in \mathbb{R}^n$:

$$\mu\|x - x'\| \leq \|\mathcal{F}(x) - \mathcal{F}(x')\| \leq \nu\|x - x'\|, \quad (1)$$

where $\|\cdot\|$ is the Euclidean norm. The bound ν controls the output sensitivity to input perturbations while μ controls the input distinguishability from different outputs. Here μ is also called the *inverse Lipschitz* bound as \mathcal{F}^{-1} exists and is $1/\mu$ -Lipschitz. For applications involving uncertainty estimation, this prevents the output from being unnecessarily invariant to the semantically meaningful changes in the input Liu et al. (2020). The ratio $\tau := \nu/\mu$ is called *distortion* Liang et al. (2023), which is the upper bound of the condition number of the Jacobian matrix of \mathcal{F} . A larger distortion implies more expressive flexibility in the model.

In this paper we argue that the bi-Lipschitz property is also useful for learning of surrogate loss (or reward) functions. Given some input/output pairs of a loss function, the objective is to learn a function which matches the observed data and is “easy to optimize” in some sense. This problem appears in many areas, including Q-learning with continuous action spaces, see e.g. Gu et al. (2016); Amos et al. (2017); Ryu et al. (2019), learning reward models in inverse reinforcement learning Arora and Doshi (2021), and data-driven surrogate losses for engineering process optimization Cozad et al. (2014); Misener and Biegler (2023). An important contribution was the input convex neural network (ICNN) Amos et al. (2017). However, the requirement of input convexity could be too strong in many applications.

1.1 Contribution

- We propose a novel strongly monotone and Lipschitz residual layer of the form $\mathcal{F}(x) = \mu x + \mathcal{H}(x)$. For the nonlinear block \mathcal{H} , we introduce a new architecture – *feed-through network* (FTN), which takes a multi-layer perceptron (MLP) as its backbone and adds connections from each hidden layer to the input and output variables. For

deep networks, this architecture can improve the model expressivity without suffering from vanishing gradients. We establish the end-to-end *strong monotonicity* (a special case of inverse Lipschitzness) and Lipschitzness for \mathcal{F} via the integral quadratic constraint (IQC) framework Megretski and Rantzer (1997), which has recently been shown to enable very tight Lipschitz bounds for network analysis Fazlyab et al. (2019) and synthesis Araujo et al. (2023); Wang and Manchester (2023), see also the toy example in Figure 1.

- We formulate the model inversion \mathcal{F}^{-1} as a three-operator splitting problem, which admits a numerically efficient solver Davis and Yin (2017).
- We introduce a new scalar-output network $f : \mathbb{R}^n \rightarrow \mathbb{R}$, which we call a *Polyak-Lojasiewicz* network (or PLNet) since it satisfies the condition of the same name Polyak (1963); Lojasiewicz (1963). It consists of a bi-Lipschitz network composed with a quadratic potential, and automatically satisfies favourable properties for surrogate loss learning, in particular a unique global optimum which is efficiently computable.

1.2 Related work

Bi-Lipschitz invertible layer. In the literature, there are two types of invertible layers closely related to our models. The first is the invertible residual layer $\mathcal{F}(x) = x + \mathcal{H}(x)$ Chen et al. (2019); Behrmann et al. (2019), where the nonlinear block \mathcal{H} is a shallow network with Lipschitz bound of $c < 1$. In Perugachi-Diaz et al. (2021), \mathcal{H} is further extended to a deep MLP. It is easy to show that \mathcal{F} is $(1 - c)$ -inverse Lipschitz and $(1 + c)$ -Lipschitz. In both cases, the Lipschitz regularization is via spectral normalization Miyato et al. (2018), which we observe to be very conservative (see Figure 1). Alternatively, bi-Lipschitz \mathcal{F} can be defined by an implicit equation Lu et al. (2021); Ahn et al. (2022). However, these require an iterative solver for both the forward and inverse model inference. In contrast, our model has an explicit forward pass and iterative solution is only required for the inverse.

IQC-based Lipschitz estimation and training. In Fazlyab et al. (2019), the IQC framework of Megretski and Rantzer (1997) was first applied to obtain accurate Lipschitz bound estimation of deep networks with slope-restricted activations. Direct (i.e. unconstrained) parameterizations based on IQC were

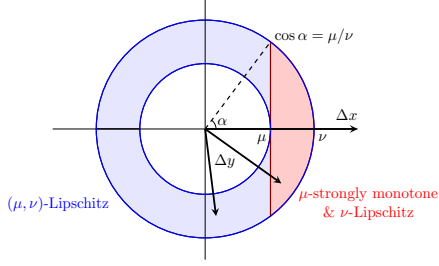


Figure 2: This figure depicts the possible ranges of $\Delta y = \mathcal{F}(x') - \mathcal{F}(x)$ on \mathbb{R}^2 for a given $\Delta x = x' - x$. The ring (blue area) is for (μ, ν) -Lipschitz \mathcal{F} while the half moon (red area) is for a μ -strongly monotone and ν -Lipschitz \mathcal{F} . The largest angle between Δx and Δy satisfies $\cos \alpha = \tau^{-1}$ with $\tau = \nu/\mu$ as the distortion.

proposed in Revay et al. (2020) for deep equilibrium networks, in Araujo et al. (2023) for residual networks, for deep MLPs and CNNs in Wang and Manchester (2023), and recurrent models in Revay et al. (2023). It was pointed out by Havens et al. (2023) that many recent Lipschitz model parameterizations Meunier et al. (2022); Prach and Lampert (2022); Araujo et al. (2023); Wang and Manchester (2023) are special cases of Revay et al. (2020). In a recent work Pauli et al. (2024), the IQC-based Lipschitz estimation was recently extended to more general activations such as GroupSort and MaxMin. All of these are for one-sided (upper) Lipschitzness, whereas our work applies the IQC framework for monotonicity and bi-Lipschitzness.

Surrogate constraint learning. Liang et al. (2023) considers the problem of learning a surrogate constraint set. The basic idea is to (i) learn a minimum *distortion* homeomorphic mapping between the non-convex constraint set \mathbb{X} and a unit ball \mathbb{B} using an INN \mathcal{F} , and then (ii) perform a simple bisection operation to find $y \in \mathbb{B}$ so that its inverse $\mathcal{F}^{-1}(y)$ is feasible w.r.t. \mathbb{X} with minor distortion-induced optimality loss. The distortion estimation in their work is based on data samples while our work offers certified distortion bounds.

2 Preliminaries

We give some definitions for a mapping $\mathcal{F} : \mathbb{R}^n \rightarrow \mathbb{R}^n$.

Definition 2.1. \mathcal{F} is said to be **μ -strongly monotone** with $\mu > 0$ if for all $x, x' \in \mathbb{R}^n$ we have

$$\langle \mathcal{F}(x) - \mathcal{F}(x'), x - x' \rangle \geq \mu \|x - x'\|^2, \quad (2)$$

where $\langle \cdot, \cdot \rangle$ is the Euclidean inner product: $\langle a, b \rangle =$

$a^\top b$. \mathcal{F} is **monotone** if the above condition holds for $\mu = 0$.

Definition 2.2. \mathcal{F} is said to be **ν -Lipschitz** with $\nu > 0$ if

$$\|\mathcal{F}(x) - \mathcal{F}(x')\| \leq \nu \|x - x'\|, \quad \forall x, x' \in \mathbb{R}^n.$$

\mathcal{F} is said to be **μ -inverse Lipschitz** with $\mu > 0$ if

$$\|\mathcal{F}(x) - \mathcal{F}(x')\| \geq \mu \|x - x'\|, \quad \forall x_1, x_2 \in \mathbb{R}^n.$$

\mathcal{F} is said to be **bi-Lipschitz** with $\nu \geq \mu > 0$, or simply (μ, ν) -Lipschitz, if it is μ -inverse Lipschitz and ν -Lipschitz.

For any (μ, ν) -Lipschitz mapping \mathcal{F} , its inverse \mathcal{F}^{-1} is well-defined and $(1/\nu, 1/\mu)$ -Lipschitz Yeh (2006). By the Cauchy–Schwarz inequality, strong monotonicity is a special case of inverse Lipschitzness, see Figure 2. A notable difference between monotonicity and bi-Lipschitzness is their composition behaviour. Given two bi-Lipschitz mappings $\mathcal{F}_1, \mathcal{F}_2$, their composition $\mathcal{F} = \mathcal{F}_2 \circ \mathcal{F}_1$ is also bi-Lipschitz with bound of $(\mu_1 \mu_2, \nu_1 \nu_2)$ where (μ_1, ν_1) and (μ_2, ν_2) are the bi-Lipschitz bounds of \mathcal{F}_1 and \mathcal{F}_2 , respectively. However, given two strongly monotone $\mathcal{F}_1, \mathcal{F}_2$ with monotonicity bounds μ_1, μ_2 , the composition $\mathcal{F} = \mathcal{F}_2 \circ \mathcal{F}_1$ does *not* need to be strongly monotone. However, it is still $\mu_1 \mu_2$ -inverse Lipschitz.

Definition 2.3. \mathcal{F} satisfies a **distortion bound** τ with $\tau \geq 1$ if \mathcal{F} is (μ, ν) -Lipschitz with $\tau = \nu/\mu$.

For example, an invertible affine mapping $\mathcal{F}(x) = Px + q$ has a distortion bound of κ , the condition number of P . An orthogonal mapping (i.e., $P^\top P = I$) has the smallest possible model distortion $\tau = 1$. Distortion bounds satisfy a composition property, i.e., if $\mathcal{F}_1, \mathcal{F}_2$ have distortion bound of τ_1, τ_2 , then $\mathcal{F}_2 \circ \mathcal{F}_1$ satisfies a distortion bound of $\tau_1 \tau_2$. Both \mathcal{F} and \mathcal{F}^{-1} have the same distortion.

3 Monotone and bi-Lipschitz Networks

In this section we first present the main contribution: construction of μ -strongly monotone and ν -Lipschitz residual layers of the form $\mathcal{F}(x) = \mu x + \mathcal{H}(x)$. Then, we use it to construct bi-Lipschitz networks by composition with orthogonal layers.

3.1 Feed-through network

For the nonlinear block \mathcal{H} , we introduce a network architecture, called *feed-through network* (FTN), which

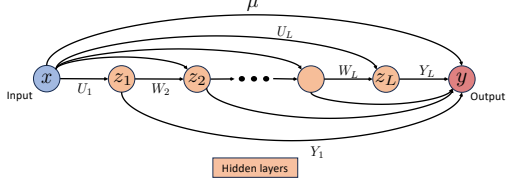


Figure 3: The proposed invertible residual network $\mathcal{F}(x) = \mu x + \mathcal{H}(x)$ where the nonlinear block \mathcal{H} is a feed-through network, whose hidden layers are directly connected to the input and output.

takes an MLP as its backbone and then connects each hidden layer to input and output variables, see Figure 3. To be specific, the residual layer $\mathcal{F}(x) = \mu x + \mathcal{H}(x)$ can be written as

$$\begin{aligned} z_k &= \sigma(W_k z_{k-1} + U_k x + b_k), \quad z_0 = 0 \\ y &= \mu x + \sum_{k=1}^L Y_k z_k + b_y \end{aligned} \quad (3)$$

where $z_k \in \mathbb{R}^{m_k}$ are the hidden variables, U_k, W_k, Y_k and b_k, b_y are the learnable weights and biases, respectively. Throughout the paper we assume that the activation σ is a scalar nonlinearity with slope restricted in $[0, 1]$, which is satisfied (possibly with rescaling) by common activation functions such as ReLU, smoothed/leaky ReLU, tanh, and sigmoid.

Remark 3.1. FTN contains both short paths $x \rightarrow y$ and $x \rightarrow z_i \rightarrow y$ preventing vanishing gradients, as well as long paths $x \rightarrow z_i \rightarrow \dots \rightarrow z_j \rightarrow y$ improving model expressivity (see Figure 3).

3.2 SDP conditions for monotonicity and Lipschitzness

We rewrite \mathcal{F} in a compact form:

$$z = \sigma(Wz + Ux + b), \quad y = \mu x + Yz + b_y \quad (4)$$

where $z = [z_1^\top \dots z_L^\top]^\top$, $b = [b_1^\top \dots b_L^\top]^\top$, and

$$\begin{aligned} W &= \begin{bmatrix} 0 & & & \\ W_2 & 0 & & \\ & \ddots & \ddots & \\ & & W_L & 0 \end{bmatrix}, \quad U = \begin{bmatrix} U_1 \\ U_2 \\ \vdots \\ U_L \end{bmatrix}, \\ Y &= [Y_1 \quad Y_2 \quad \dots \quad Y_L]. \end{aligned}$$

We first establish strong monotonicity and Lipschitzness for \mathcal{F} via semidefinite programming (SDP) conditions.

Theorem 3.2. \mathcal{F} is μ -strongly monotone and ν -Lipschitz if there exists a $\Lambda \in \mathbb{D}_+^m$, where \mathbb{D}_+^m is the set of positive diagonal matrices, such that the following conditions hold:

$$Y = U^\top \Lambda, \quad 2\Lambda - \Lambda W - W^\top \Lambda \succeq \frac{2}{\gamma} Y^\top Y \quad (5)$$

where $\gamma = \nu - \mu > 0$.

Remark 3.3. The above conditions are obtained by applying the IQC theory Megretski and Rantzer (1997) to (4).

3.3 Model parameterization

Let Θ be the set of all $\theta = \{\Lambda, U, W, Y\}$ such that Condition (5) holds. Since it is generally not scalable to train a model with SDP constraints, we instead construct a *direct parameterization*, i.e. both unconstrained and complete:

Definition 3.4. A *direct parameterization* of a constraint set Θ is a differentiable mapping \mathcal{M} such that for any $\phi \in \mathbb{R}^N$ we have $\mathcal{M}(\phi) \in \Theta$, and the image of \mathbb{R}^N maps onto Θ , i.e. $\mathcal{M}(\mathbb{R}^N) = \Theta$.

A direct parameterization allows us to replace a constrained optimization over $\theta \in \Theta$ with an unconstrained optimization over $\phi \in \mathbb{R}^N$, using standard first-order optimization algorithms such as SGD or ADAM Kingma and Ba (2015).

We now construct the direct parameterization, see Appendix A for details. First, we introduce the free parameter

$$\phi = \{d, F_k^a, F_k^b, F^q, F^*\}, \quad k = 1, \dots, L$$

where $d \in \mathbb{R}^m$, $F_k^a \in \mathbb{R}^{m_k \times m_k}$, $F_k^b \in \mathbb{R}^{m_{k-1} \times m_k}$, $F^q \in \mathbb{R}^{m \times n}$ and $F^* \in \mathbb{R}^{n \times n}$ with $m_0 = 0$. Then, we compute some intermediate variables $\Psi = \text{diag}(e^\psi)$ and

$$\begin{bmatrix} A_k^\top \\ B_k^\top \end{bmatrix} = \text{Cayley} \left(\begin{bmatrix} F_k^a \\ F_k^b \end{bmatrix} \right), \quad \begin{bmatrix} Q \\ \star \end{bmatrix} = \text{Cayley} \left(\begin{bmatrix} F^q \\ F^* \end{bmatrix} \right)$$

where Cayley : $\mathbb{R}^{n \times p} \rightarrow \mathbb{R}^{n \times p}$ with $n \geq p$ is defined by

$$J = \text{Cayley} \left(\begin{bmatrix} G \\ H \end{bmatrix} \right) := \begin{bmatrix} (I + Z)(I - Z)^{-1} \\ -2V(I - Z)^{-1} \end{bmatrix} \quad (6)$$

where $Z = G^\top - G + H^\top H$. It is easy to verify that $J^\top J = I$ for any $G \in \mathbb{R}^{p \times p}$ and $H \in \mathbb{R}^{(n-p) \times p}$. The Cayley transformation has been applied to construct orthogonal layers Helfrich et al. (2018); Li et al. (2020); Trockman and Kolter (2021). By introducing $V_k =$

$2B_k A_{-1}^\top$ and $S_k = A_k Q_k - B_k Q_{k-1}$ with $B_1 = 0$, $Q_0 = 0$ and $Q = [Q_1^\top \cdots Q_L^\top]^\top$, we finally construct $\theta = \mathcal{M}(\phi)$ as follows:

$$\begin{aligned} U_k &= \sqrt{2\gamma} \Psi_k^{-1} S_k, \quad W_k = \Psi_k^{-1} V_k \Psi_{k-1}, \\ Y_k &= \sqrt{\frac{\gamma}{2}} S_k^\top \Psi_k, \quad \Lambda_k = \frac{1}{2} \Psi_k^2. \end{aligned} \quad (7)$$

Proposition 3.5. *The model parameterization \mathcal{M} defined in (7) is a direct parameterization for the set Θ , i.e. all models (4) satisfying Condition (5).*

This means that we can learn the free parameter ϕ using first-order methods without any loss of model expressivity.

The construction is now done, but we note that Ψ_k is shared between layers k and $k+1$. To have a modular implementation, we introduce the following scaled variables $\hat{z} = \Psi z$ and bias $\hat{b} = \Psi b$. Then, (4) can be rewritten as follows

$$\hat{z} = \hat{\sigma}(V\hat{z} + \sqrt{2\gamma}Sx + \hat{b}), \quad y = \mu x + \sqrt{\gamma/2}S^\top \hat{z} + b_y \quad (8)$$

where $\hat{\sigma}(x) := \Psi\sigma(\Psi^{-1}x)$ is a $(0, 1)$ -Lipschitz layer with learnable scaling Ψ . The weight matrices are

$$S = \begin{bmatrix} S_1 \\ S_2 \\ \vdots \\ S_L \end{bmatrix}, \quad V = \begin{bmatrix} 0 & & & \\ V_2 & 0 & & \\ & \ddots & \ddots & \\ & & V_L & 0 \end{bmatrix}. \quad (9)$$

3.4 Bi-Lipschitz networks

By composing strongly monotone and Lipschitz layers, we can obtain bi-Lipschitz networks (referred as BiLip-Nets):

$$\mathcal{G} = \mathcal{O}_{K+1} \circ \mathcal{F}_K \circ \mathcal{O}_K \circ \mathcal{F}_{K-1} \circ \cdots \circ \mathcal{O}_2 \circ \mathcal{F}_1 \circ \mathcal{O}_1 \quad (10)$$

where $\mathcal{O}_k(x) = P_k x + q_k$ with $P_k^\top P_k = I$ is an orthogonal layer and \mathcal{F}_k is a μ_k -strongly monotone and ν_k -Lipschitz layer (8). By the composition rule, the above BiLipNet is (μ, ν) -Lipschitz with $\mu = \prod_{k=1}^L \mu_k$ and $\nu = \prod_{k=1}^L \nu_k$. The orthogonal matrix P can be parameterized via the Cayley transformation (6) or Householder transformation Singla et al. (2022). Since the distortion of \mathcal{O}_k is 1, it can improve network expressivity without increasing model distortion.

In some applications, e.g., normalising flows Dinh et al. (2015); Papamakarios et al. (2021), we need to compute the inverse of \mathcal{G} , which can be done in a backward manner:

$$\mathcal{G}^{-1}(y) = \mathcal{O}_1^{-1} \circ \mathcal{F}_1^{-1} \circ \cdots \circ \mathcal{O}_K^{-1} \circ \mathcal{F}_K^{-1} \circ \mathcal{O}_{K+1}^{-1}(y), \quad (11)$$

where \mathcal{O}_k has an explicit inverse $\mathcal{O}_k^{-1}(y) = P_k^\top (y - q_k)$. Computing the inverse $\mathcal{F}_k^{-1}(y)$ requires an iterative solver, which will be addressed in the next section.

Partially bi-Lipschitz networks. A neural network $\tilde{\mathcal{G}} : \mathbb{R}^n \times \mathbb{R}^l \rightarrow \mathbb{R}^n$ is said to be *partially bi-Lipschitz* if for any fixed value of $p \in \mathbb{R}^l$, the mapping $y = \tilde{\mathcal{G}}(x; p)$ is a (μ, ν) -Lipschitz network from x to y . We can construct such mappings via $\tilde{\mathcal{G}}(x; p) = \mathcal{G}_{h(p)}(x)$ where \mathcal{G}_ϕ is a (μ, ν) -Lipschitz network for any free parameter $\phi \in \mathbb{R}^N$ and $h : p \rightarrow \phi$ is a new learnable function. Since the dimension of ϕ is often very high, a practical approach is to make ϕ partially depend on p . For instance, we can learn p -dependent bias via an MLP with weight matrices independent of p .

4 Model inverse via operator splitting

In this section we give an efficient algorithm to compute $\mathcal{F}^{-1}(y)$ where \mathcal{F} is a μ -strongly monotone and ν -Lipschitz layer (8). First, we write its model inverse \mathcal{F}^{-1} as

$$\begin{aligned} \hat{z} &= \hat{\sigma} \left(\left(V - \frac{\gamma}{\mu} S S^\top \right) \hat{z} + b_z \right) \\ x &= \frac{1}{\mu} (y - b_y - \sqrt{\gamma/2} S^\top \hat{z}) \end{aligned} \quad (12)$$

with $b_z = \sqrt{2\gamma}/\mu S(y - b_y) + \hat{b}$. Both \mathcal{F} and \mathcal{F}^{-1} can be treated as special cases of *equilibrium networks* Revay et al. (2020). The difference is that \mathcal{F} has an explicit formula due to the strictly lower-triangular V while \mathcal{F}^{-1} is an implicit equation as $S S^\top$ is a full matrix. A natural question for (12) is its **well-posedness**, i.e., for any $y \in \mathbb{R}^n$, does there exist a unique $\hat{z} \in \mathbb{R}^m$ satisfying (12)?

Proposition 4.1. *\mathcal{F}^{-1} is well-posed if V, S are given by (9).*

A simple way to compute \mathcal{F}^{-1} is the forward step method (**FSM**) see, e.g., Ryu and Boyd (2016)

$$x^{k+1} = x^k - \alpha(\mathcal{F}(x^k) - y) \quad (13)$$

which has a convergence rate of $1 - \mu^2/\nu^2$ if $\alpha = \mu/\nu^2$. In Winston and Kolter (2020); Revay et al. (2020), certain classes of equilibrium networks were solved via two-operator splitting problems. We follow a similar strategy, but our structure requires a three-operator splitting, see Proposition 4.2 with background in Appendix B. To state the result, we first recall that for a monotone and 1-Lipschitz activation function, there

exists a proper convex function $f : \mathbb{R}^n \rightarrow \mathbb{R}$ satisfying $\hat{\sigma}(\cdot) = \mathbf{prox}_f^1(\cdot)$ with

$$\mathbf{prox}_f^\alpha(x) = \arg \min_{z \in \mathbb{R}^n} 1/2\|x - z\|^2 + \alpha f(z).$$

A list of f for popular activations is given in Appendix B.1. In particular, the ReLU activation satisfies $\hat{\sigma}(\cdot) = \mathbf{prox}_f^\alpha(\cdot)$ for any $\alpha > 0$, which simplifies implementation of the proposed algorithm.

Proposition 4.2. *Finding a solution $\hat{z} \in \mathbb{R}^m$ to (12) is equivalent to finding a zero to the three-operator splitting problem $0 \in \mathcal{A}(z) + \mathcal{B}(z) + \mathcal{C}(z)$ where $\mathcal{A}, \mathcal{B}, \mathcal{C}$ are monotone operators defined by*

$$\mathcal{A}(z) = (I - V)z - b_z, \mathcal{B}(z) = \partial f(z), \mathcal{C}(z) = \frac{\gamma}{\mu} S S^\top z$$

where f satisfies $\hat{\sigma}(\cdot) = \mathbf{prox}_f^1(\cdot)$.

For three-operator problems, the Davis-Yin splitting algorithm (**DYS**) Davis and Yin (2017) can be applied, obtaining the following fixed-point iteration:

$$\begin{aligned} z^{k+1/2} &= \mathbf{prox}_f^\alpha(u^k) \\ u^{k+1/2} &= 2z^{k+1/2} - u^k \\ z^{k+1} &= R_{\mathcal{A}}(u^{k+1/2} - \alpha \mathcal{C}(z^{k+1/2})) \\ u^{k+1} &= u^k + z^{k+1} - z^{k+1/2} \end{aligned} \tag{14}$$

where $R_{\mathcal{A}}(v) = ((1 + \alpha)I - \alpha V)^{-1}(v + \alpha b_z)$. Since V is strictly lower triangular, we can solve $R_{\mathcal{A}}(v)$ using forward substitution. Furthermore, we can show that (14) is guaranteed to converge with $\alpha \in (0, \frac{1}{\tau-1})$, where τ is the model distortion.

5 Polyak-Łojasiewicz Networks

We call a network $f : \mathbb{R}^n \rightarrow \mathbb{R}$ a *Polyak-Łojasiewicz (PL) network*, or PLNet for short, if it satisfies the following PL condition (Polyak, 1963; Łojasiewicz, 1963):

$$\frac{1}{2}\|\nabla_x f(x)\|^2 \geq m(f(x) - \min_x f(x)), \quad \forall x \in \mathbb{R}^n, \tag{15}$$

where $m > 0$. The PL condition is significant in optimization since it is weaker than convexity, but still implies that gradient methods converge to a global minimum with a linear rate (Karimi et al., 2016), making PL networks a promising candidate for learning a surrogate loss models.

Proposition 5.1. *If \mathcal{G} is μ -inverse Lipschitz, then*

$$f(x) = \frac{1}{2}\|\mathcal{G}(x)\|^2 + c, \quad c \in \mathbb{R} \tag{16}$$

is a PL network with $m = \mu^2$.

By construction, f has a global minimum value of c , obtained uniquely at the point $x^* = \mathcal{G}^{-1}(0)$.

Remark 5.2. We can relax the quadratic assumption: $f(x) = h(\mathcal{G}(x))$ is a PL network if $h : \mathbb{R}^n \rightarrow \mathbb{R}$ is strongly convex Karimi et al. (2016).

Remark 5.3. For parametric optimization problem, one can learn a surrogate loss via $f(x; p) = 1/2\|\tilde{\mathcal{G}}(x; p)\|^2 + c$ where $p \in \mathbb{R}^m$ is the problem-specific parameter and $\tilde{\mathcal{G}}$ is a partially bi-Lipschitz network.

Remark 5.4. Any non-empty sub-level set $\mathbb{L}_\alpha = \{x : f(x) < \alpha\}$ is homeomorphic to a unit ball, making PL networks suitable for learning Lyapunov functions of stable dynamical systems Wilson Jr (1967).

Computing global optimum of a PL network If \mathcal{G} is also ν -Lipschitz (i.e., it is (μ, ν) -bi-Lipschitz) then f has a unique global optimum $x^* = \mathcal{G}^{-1}(0)$ with \mathcal{G}^{-1} given by (11). This can be efficiently computed by analytical inversion orthogonal layers and applying the DYS algorithm (14) to monotone and Lipschitz layers.

Limitations of gradient descent for finding global optimum. An alternative way to compute the global optimum x^* is the standard gradient descent (GD) method $x^{k+1} = x^k - \alpha \nabla_x f(x^k)$. If $\nabla_x f$ is L -Lipschitz, then the above GD solver with $\alpha = 1/L$ has a linear global convergence rate of $1 - m/L$ with $m = \mu^2$ (Karimi et al., 2016). However, this method has two drawbacks. First, the gradient function $\nabla_x f$ may not be globally Lipschitz, see Example 5.5. Secondly, even if a global Lipschitz bound exists, it is still hard to obtain a good estimation of L for high-dimensional problems.

Example 5.5. Consider a scalar function $f(x) = 0.5g^2(x)$ with $g(x) = 2x + \sin x$. Then, $\partial f/\partial x = (2 + \cos x)(2x + \sin x)$ is not globally Lipschitz due to the term $2x \cos x$.

6 Experiments

Here we present experiments which explore the expressive quality of the proposed models, regularisation via model distortion, and performance of the DYS solution method.

6.1 Uncertainty quantification via neural Gaussian process

As shown in Liu et al. (2020), a model's ability to quantify the distance of a testing example from training data

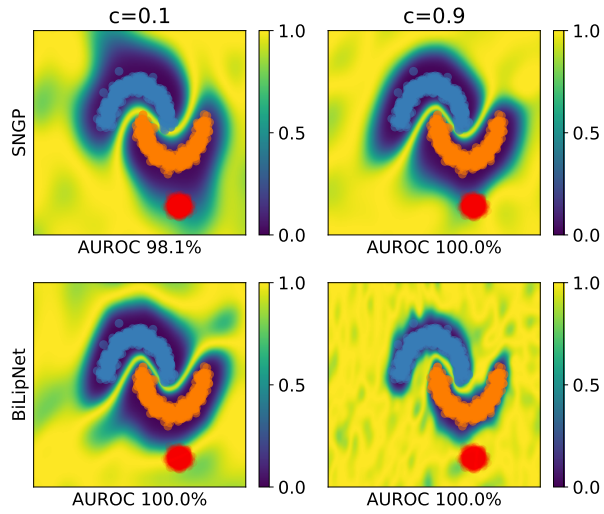


Figure 4: The uncertainty plot of neural Gaussian process with different models for the same bi-Lipschitz bounds. For the case with small distortion, our model can still distinguish the train and OOD data, achieving similar results of SNGP with large distortion.

is a necessary condition for neural networks to achieve high quality uncertainty estimation. The distance-awareness can be achieved by imposing bi-Lipschitz smoothness for each residual layer $\mathcal{F}(x) = x + \mathcal{H}(x)$ and replace the output layer with a Gaussian process layer. The bi-Lipschitz regularization is done by imposing Lipschitz bound of $0 < c < 1$ for \mathcal{H} via spectral normalization. The resulting model is called Spectral-normalized Neural Gaussian Process (SNGP).

We replace the hidden space mapping with our bi-Lipschitz models and keep the same output layer. We compare our (μ, ν) -Lipschitz network to a 3-layer i-ResNet under the same bi-Lipschitz bound constraint, i.e., $\mu = (1-c)^3$ and $\nu = (1+c)^3$. Empirical results on the two-moon dataset are shown in Figure 4. For the lower-distortion case (i.e., small $c = 0.1$), SNGP fails to completely separate the train and out-of-distribution (OOD) data due to its loose Lipschitz bound. Our model can distinguish the OOD examples from training dataset and the uncertainty surface is close to the SNGP with much higher distortion ($c = 0.9$). As the model distortion increases, our model can have an uncertainty surface very close the dataset. The uncertainty surface of SNGP does not change much form $c = 0.1$ to $c = 0.9$, see Figure 4 and additional results in Appendix D.2.

6.2 Surrogate loss learning

We explore the PL Network’s performance with the Rosenbrock function $r(x, y) = 1/200(x - 1)^2 + 0.5(y - x^2)^2$ and its higher-dimensional generalisations. The classical Rosenbrock function is a non-convex function which has a unique global minimum point $(1, 1)$. It has been widely used as a test example for various of gradient-descent based optimization algorithms due to the fact that its Hessian near the optimum is very poorly conditioned. We also consider learning a surrogate loss for the sum of the Rosenbrock function and a 2D sinewave function, chosen such that the overall loss still has a unique global minimum at $(1, 1)$ while having many local minima, see Appendix D.1.

We learned models based on the form (16) where \mathcal{G} is parameterized by MLP, i-ResNet Behrmann et al. (2019), i-DenseNet Perugachi-Diaz et al. (2021) and the proposed BiLipNet (10). We also trained the ICNN, a scalar-output model which is convex w.r.t. inputs Amos et al. (2017).

Based on the results in Figure 7, we have the following observations. The unconstrained MLP can achieve very small test errors. However, it has many local minima near the valley $y = x^2$ since it is not inverse Lipschitz. This phenomena is more easily visible for the Rosenbrock+Sine case but also occurs in the plain Rosenbrock case. The ICNN model has a unique global minimum but the fitting error is large as its sub-level sets are convex. For i-DenseNet, the sub-level sets become mildly non-convex but their bi-Lipschitz bound is quite conservative, so they do not capture the overall shape. In contrast, our proposed BiLipNet is more flexible and captures the non-convex shape while maintaining a unique global minimum. Additional results are in Appendix D.2.

Partially PL network. We fit a parameterized Rosenbrock function: $r(x, y; p) = 1/200(x - a)^2 + 0.5(y - bx^2)^2$ with $p = (a, b)$ by learning a partially PL network (see Remark 5.3.) with p -dependent bias terms. The results in Figure 8 indicate that the approach can be effective even if only bias terms are modified by p , and not weights.

High-dimensional case. We now turn to scalability of the approach to higher-dimensional problems and analyse convergence of the DYS method for computing the global minimum. We apply the approach to a

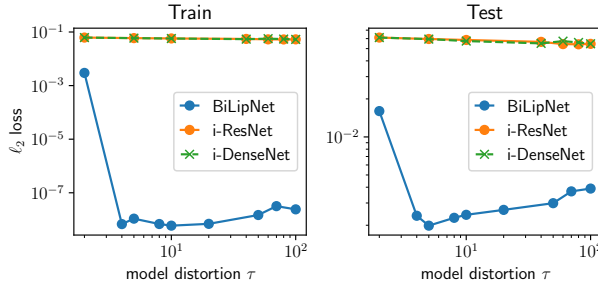


Figure 5: Surrogate loss learning for 20-dimensional Rosenbrock function. Comparison of training and test error vs model distortion for PLNet with different bi-Lipschitz models.

$N=20$ -dimensional version of the Rosenbrock function:

$$r(x) = \frac{1}{N-1} \sum_{i=1}^{N-1} r(x_i, x_{i+1}) \quad (17)$$

which has a global minimum of zero at $x = (1, 1, \dots, 1)$ but is non-convex and has spurious local minima Kok and Sandrock (2009).

We sample 10,000 training points uniformly over $[-2, 2]^{20}$. Note that, in contrast to the 2D example above, this is very sparse sampling of 20-dimensional space. We fit PL-networks of the form (16) with \mathcal{G} constructed as the proposed BiLipNet as well as i-Resnet and i-DenseNet for comparison.

A comparison of train and test error vs model distortion is shown in Figure 5. It can be seen that our proposed BiLipNet model achieves far better fits than iResNet Behrmann et al. (2021) and iDenseNet Perugachi-Diaz et al. (2021), which can not achieve small training error for any value of the distortion parameter. Furthermore, for our network, the distortion parameter appears to act as an effective regularizer. Note that the best test error occurs after training error drops to near zero ($\sim 10^{-8}$) but distortion is still relatively small.

Solver comparison. Given the surrogate loss function learned by BiLipNet, we now compare methods to compute the location of its global minimum. In Figure 6 we compare the proposed DYS solver to the FSM algorithm (13) and Adam Kingma and Ba (2015) applied directly to the surrogate loss. We take two values of the distortion parameter: $\tau = 5$ (optimal) and $\tau = 50$. In both cases, the proposed DYS method converges significantly faster than the alternatives, and

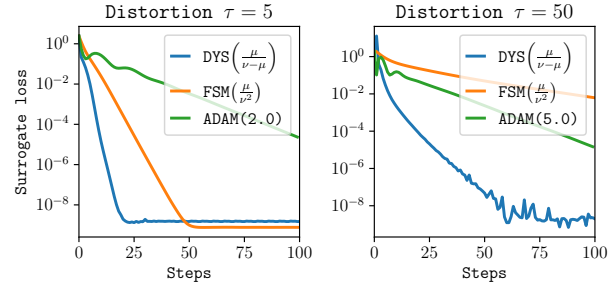


Figure 6: Solver comparison for finding the global minimum of a PLNet. We try a range of rates $[0.1, 0.5, 1.0, 2.0, 5.0]$ for ADAM and present the best result. The proposed back solve method with DYS algorithm (14) converges much faster than ADAM applied to f or back solve method with FSM algorithm (13).

the results illustrate an additional benefit of regularising via distortion, besides improving the test error: the $\tau = 5$ case converges significantly faster than $\tau = 50$.

At the computed point $x^* = \mathcal{G}^{-1}(0)$ for the $\tau = 5$ case, the true function (17) takes a value of $r(x^*) = 0.041$. This is more than an order of magnitude better than the smallest value of $r(x)$ over the training data, which ranged over $[0.475, 6.532]$, indicating that some useful structure has been learned.

7 Conclusion

In this paper we have introduced a “feed-through” layer with certified bounds for strong monotonicity and Lipschitzness. By composing with orthogonal layers we obtain a bi-Lipschitz network structure (BiLipNet) which has much tighter bounds than those based on spectral normalization.

Building on these models, we have introduced the PLNet which is a scalar-output neural network satisfying the Polyak-Lojasiewicz condition. PLNet has many features making it suitable for learning surrogate loss functions, including as a unique global minimum and a fast algorithm to compute it.

References

Ahn, B., Kim, C., Hong, Y., and Kim, H. J. (2022). Invertible monotone operators for normalizing flows. *Advances in Neural Information Processing Systems*, 35:16836–16848.

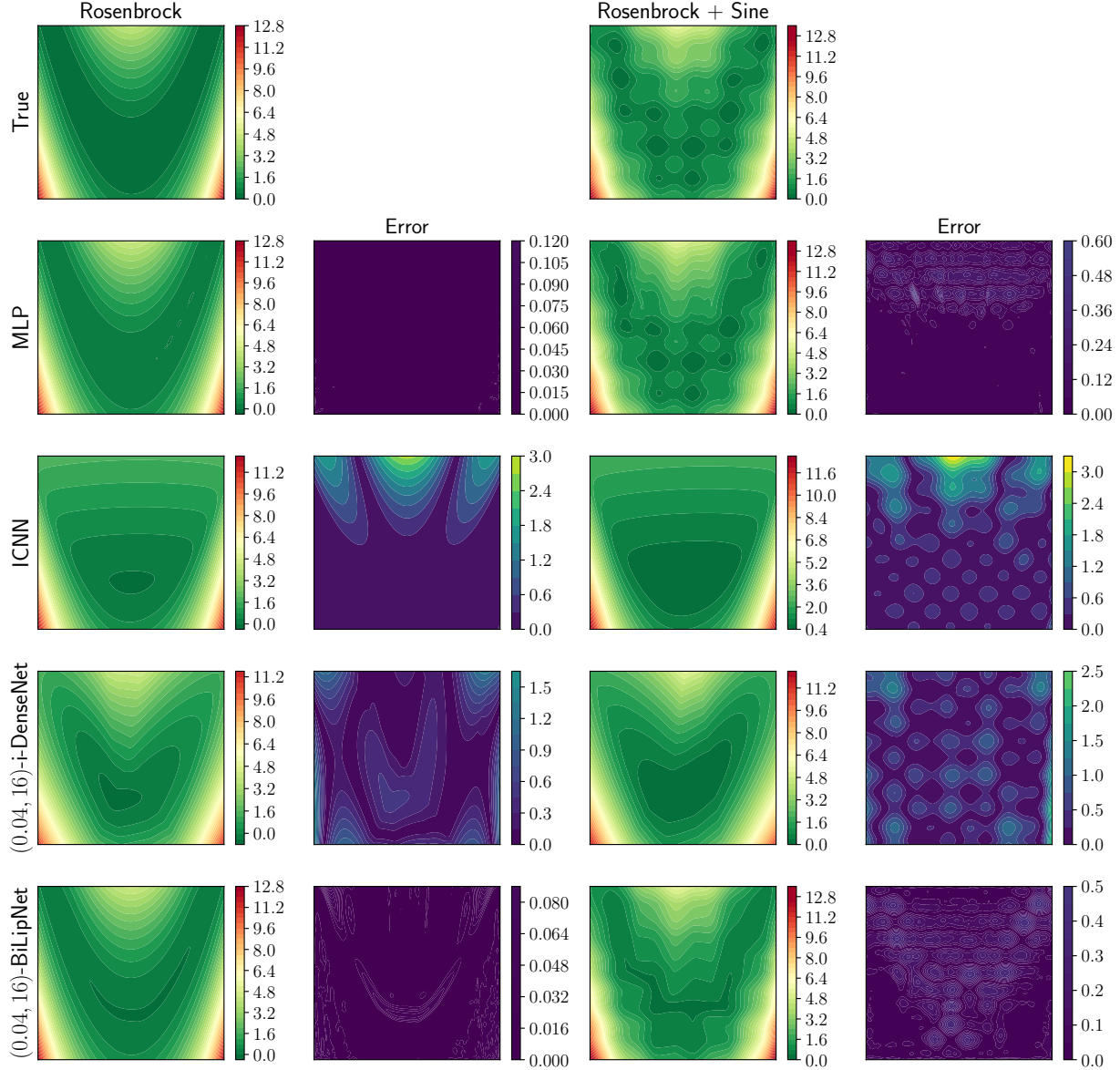


Figure 7: Learning a surrogate loss for the Rosenbrock and Rosenbrock+Sine functions, which is non-convex and has many local minima. The first row contains the true functions while the remaining rows show learned functions and errors for various surrogate loss models.

Amos, B., Xu, L., and Kolter, J. Z. (2017). Input convex neural networks. In *International Conference on Machine Learning (ICML)*, pages 146–155. PMLR.

Araujo, A., Havens, A. J., Delattre, B., Allauzen, A., and Hu, B. (2023). A unified algebraic perspective on lipschitz neural networks. In *The Eleventh International Conference on Learning Representations (ICLR)*.

Ardizzone, L., Kruse, J., Rother, C., and Köthe, U.

(2018). Analyzing inverse problems with invertible neural networks. In *International Conference on Learning Representations (ICLR)*.

Arjovsky, M., Chintala, S., and Bottou, L. (2017). Wasserstein generative adversarial networks. In *International conference on machine learning (ICML)*, pages 214–223. PMLR.

Arora, S. and Doshi, P. (2021). A survey of inverse

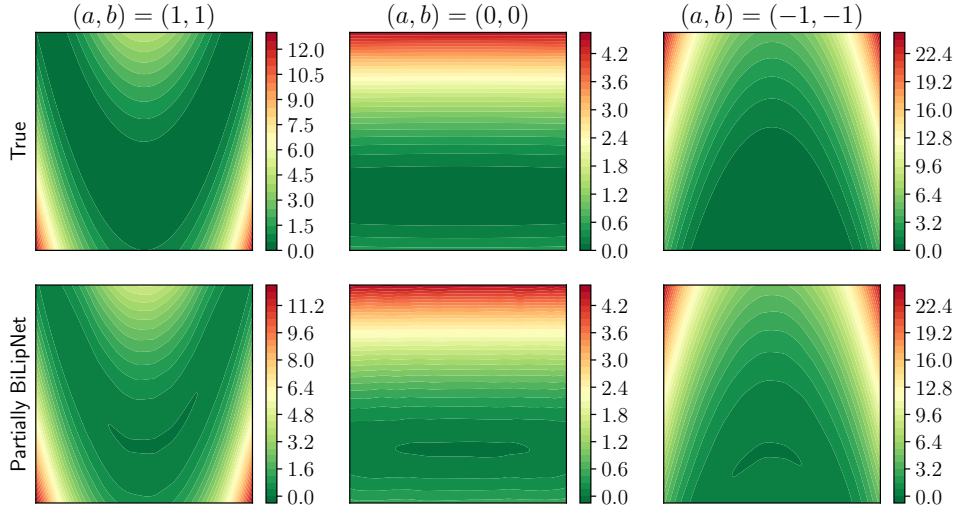


Figure 8: Learning a parameterized Rosenbrock function via a partially-PL network constructed with a partially-BiLipNet.

reinforcement learning: Challenges, methods and progress. *Artificial Intelligence*, 297:103500.

Bauer, M. and Mnih, A. (2019). Resampled priors for variational autoencoders. In *The 22nd International Conference on Artificial Intelligence and Statistics*, pages 66–75. PMLR.

Behrmann, J., Grathwohl, W., Chen, R. T., Duvenaud, D., and Jacobsen, J.-H. (2019). Invertible residual networks. In *International conference on machine learning (ICML)*, pages 573–582. PMLR.

Behrmann, J., Vicol, P., Wang, K.-C., Grosse, R., and Jacobsen, J.-H. (2021). Understanding and mitigating exploding inverses in invertible neural networks. In *International Conference on Artificial Intelligence and Statistics*, pages 1792–1800. PMLR.

Chen, R. T., Behrmann, J., Duvenaud, D. K., and Jacobsen, J.-H. (2019). Residual flows for invertible generative modeling. *Advances in Neural Information Processing Systems*, 32.

Coleman, C., Narayanan, D., Kang, D., Zhao, T., Zhang, J., Nardi, L., Bailis, P., Olukotun, K., Ré, C., and Zaharia, M. (2017). Dawnbench: An end-to-end deep learning benchmark and competition. *Training*, 100(101):102.

Cozad, A., Sahinidis, N. V., and Miller, D. C. (2014). Learning surrogate models for simulation-based optimization. *AICHE Journal*, 60(6):2211–2227.

Davis, D. and Yin, W. (2017). A three-operator splitting scheme and its optimization applications. *Set-valued and variational analysis*, 25:829–858.

Davis, T. A. (2006). *Direct methods for sparse linear systems*. SIAM.

De Cao, N., Aziz, W., and Titov, I. (2020). Block neural autoregressive flow. In *Uncertainty in artificial intelligence*, pages 1263–1273. PMLR.

Dinh, L., Krueger, D., and Bengio, Y. (2015). Nice: Non-linear independent components estimation. *ICLR Workshop Track*.

Dinh, L., Sohl-Dickstein, J., and Bengio, S. (2017). Density estimation using real nvp. In *International Conference on Learning Representations (ICLR)*.

Fazlyab, M., Robey, A., Hassani, H., Morari, M., and Pappas, G. (2019). Efficient and accurate estimation of lipschitz constants for deep neural networks. In *Advances in Neural Information Processing Systems*, pages 11427–11438.

Grathwohl, W., Chen, R. T., Bettencourt, J., and Duvenaud, D. (2019). Scalable reversible generative models with free-form continuous dynamics. In *International Conference on Learning Representations (ICLR)*.

Gu, S., Lillicrap, T., Sutskever, I., and Levine, S. (2016). Continuous deep q-learning with model-based acceleration. In *International conference on machine learning (ICML)*, pages 2829–2838. PMLR.

Gulrajani, I., Ahmed, F., Arjovsky, M., Dumoulin, V., and Courville, A. C. (2017). Improved training of wasserstein gans. *Advances in neural information processing systems*, 30.

Havens, A. J., Araujo, A., Garg, S., Khorrami, F., and Hu, B. (2023). Exploiting connections between lipschitz structures for certifiably robust deep equilibrium models. In *Thirty-seventh Conference on Neural Information Processing Systems*.

Helfrich, K., Willmott, D., and Ye, Q. (2018). Orthogonal recurrent neural networks with scaled cayley transform. In *International Conference on Machine Learning (ICML)*, pages 1969–1978. PMLR.

Ho, J., Chen, X., Srinivas, A., Duan, Y., and Abbeel, P. (2019). Flow++: Improving flow-based generative models with variational dequantization and architecture design. In *International Conference on Machine Learning (ICML)*, pages 2722–2730. PMLR.

Huang, C.-W., Krueger, D., Lacoste, A., and Courville, A. (2018). Neural autoregressive flows. In *International Conference on Machine Learning (ICML)*, pages 2078–2087. PMLR.

Karimi, H., Nutini, J., and Schmidt, M. (2016). Linear convergence of gradient and proximal-gradient methods under the polyak-lojasiewicz condition. In *Machine Learning and Knowledge Discovery in Databases: European Conference, ECML PKDD 2016, Riva del Garda, Italy, September 19-23, 2016, Proceedings, Part I* 16, pages 795–811. Springer.

Kingma, D. P. and Ba, J. (2015). Adam: A method for stochastic optimization. In *International Conference on Learning Representations (ICLR)*.

Kingma, D. P. and Dhariwal, P. (2018). Glow: Generative flow with invertible 1x1 convolutions. *Advances in neural information processing systems*, 31.

Kobyzev, I., Prince, S. J., and Brubaker, M. A. (2020). Normalizing flows: An introduction and review of current methods. *IEEE transactions on pattern analysis and machine intelligence*, 43(11):3964–3979.

Kok, S. and Sandrock, C. (2009). Locating and Characterizing the Stationary Points of the Extended Rosenbrock Function. *Evolutionary Computation*, 17(3):437–453.

Li, J., Fang, C., and Lin, Z. (2019). Lifted proximal operator machines. In *Proceedings of the AAAI Conference on Artificial Intelligence*, volume 33, pages 4181–4188.

Li, J., Li, F., and Todorovic, S. (2020). Efficient riemannian optimization on the stiefel manifold via the cayley transform. In *International Conference on Learning Representations (ICLR)*.

Liang, E., Chen, M., and Low, S. (2023). Low complexity homeomorphic projection to ensure neural-network solution feasibility for optimization over (non-) convex set.

Liu, J., Lin, Z., Padhy, S., Tran, D., Bedrax Weiss, T., and Lakshminarayanan, B. (2020). Simple and principled uncertainty estimation with deterministic deep learning via distance awareness. *Advances in Neural Information Processing Systems*, 33:7498–7512.

Lojasiewicz, S. (1963). A topological property of real analytic subsets. *Coll. du CNRS, Les équations aux dérivées partielles*, 117(87-89):2.

Louizos, C. and Welling, M. (2017). Multiplicative normalizing flows for variational bayesian neural networks. In *International Conference on Machine Learning (ICML)*, pages 2218–2227. PMLR.

Lu, C., Chen, J., Li, C., Wang, Q., and Zhu, J. (2021). Implicit normalizing flows. In *International Conference on Learning Representations (ICLR)*.

Megretski, A. and Rantzer, A. (1997). System analysis via integral quadratic constraints. *IEEE Transactions on Automatic Control*, 42(6):819–830.

Meunier, L., Delattre, B. J., Araujo, A., and Allauzen, A. (2022). A dynamical system perspective for lipschitz neural networks. In *International Conference on Machine Learning (ICML)*, pages 15484–15500. PMLR.

Misener, R. and Biegler, L. (2023). Formulating data-driven surrogate models for process optimization. *Computers & Chemical Engineering*, 179:108411.

Miyato, T., Kataoka, T., Koyama, M., and Yoshida, Y. (2018). Spectral normalization for generative adversarial networks. In *International Conference on Learning Representations (ICLR)*.

Papamakarios, G., Nalisnick, E., Rezende, D. J., Mohamed, S., and Lakshminarayanan, B. (2021). Normalizing flows for probabilistic modeling and inference. *The Journal of Machine Learning Research*, 22(1):2617–2680.

Pauli, P., Havens, A., Araujo, A., Garg, S., Khorrami, F., Allgöwer, F., and Hu, B. (2024). Novel

quadratic constraints for extending lipsdip beyond slope-restricted activations. In *International Conference on Learning Representations (ICLR)*.

Pauli, P., Koch, A., Berberich, J., Kohler, P., and Allgöwer, F. (2021). Training robust neural networks using lipschitz bounds. *IEEE Control Systems Letters*, 6:121–126.

Perugachi-Diaz, Y., Tomczak, J., and Bhulai, S. (2021). Invertible densenets with concatenated lipswish. *Advances in Neural Information Processing Systems*, 34:17246–17257.

Polyak, B. (1963). Gradient methods for minimizing functionals (in russian). *USSR Computational Mathematics and Mathematical Physics*, 3(4):643–653.

Prach, B. and Lampert, C. H. (2022). Almost-orthogonal layers for efficient general-purpose lipschitz networks. In *European Conference on Computer Vision*, pages 350–365. Springer.

Rantzer, A. (1996). On the kalman—yakubovich—popov lemma. *Systems & control letters*, 28(1):7–10.

Revay, M., Wang, R., and Manchester, I. R. (2020). Lipschitz bounded equilibrium networks. *arXiv preprint arXiv:2010.01732*.

Revay, M., Wang, R., and Manchester, I. R. (2023). Recurrent equilibrium networks: Flexible dynamic models with guaranteed stability and robustness. *IEEE Transactions on Automatic Control*.

Russo, A. and Proutiere, A. (2021). Towards optimal attacks on reinforcement learning policies. In *2021 American Control Conference (ACC)*, pages 4561–4567. IEEE.

Ryu, E. K. and Boyd, S. (2016). Primer on monotone operator methods. *Appl. comput. math.*, 15(1):3–43.

Ryu, M., Chow, Y., Anderson, R., Tjandraatmadja, C., and Boutilier, C. (2019). Caql: Continuous action q-learning. In *International Conference on Learning Representations (ICLR)*.

Singla, S. and Feizi, S. (2021). Skew orthogonal convolutions. In *International Conference on Machine Learning (ICML)*, pages 9756–9766. PMLR.

Singla, S., Singla, S., and Feizi, S. (2022). Improved deterministic l2 robustness on cifar-10 and cifar-100. In *International Conference on Learning Representations (ICLR)*.

Trockman, A. and Kolter, J. Z. (2021). Orthogonalizing convolutional layers with the cayley transform. In *International Conference on Learning Representations (ICLR)*.

Tsuzuku, Y., Sato, I., and Sugiyama, M. (2018). Lipschitz-margin training: Scalable certification of perturbation invariance for deep neural networks. In *Advances in neural information processing systems*, pages 6541–6550.

Wang, R. and Manchester, I. (2023). Direct parameterization of lipschitz-bounded deep networks. In *International Conference on Machine Learning (ICML)*, pages 36093–36110. PMLR.

Ward, P. N., Smofsky, A., and Bose, A. J. (2019). Improving exploration in soft-actor-critic with normalizing flows policies. *ICML Workshop on Invertible Neural Networks and Normalizing Flows*.

Wilson Jr, F. (1967). The structure of the level surfaces of a lyapunov function.

Winston, E. and Kolter, J. Z. (2020). Monotone operator equilibrium networks. *Advances in neural information processing systems*, 33:10718–10728.

Yeh, J. (2006). *Real analysis: theory of measure and integration second edition*. World Scientific Publishing Company.

A Model Parameterization

Model parameterization is a mapping $\mathcal{M} : \phi \rightarrow \theta$ where $\phi \in \mathbb{R}^N$ is a free learnable parameter while θ includes the model weights $U \in \mathbb{R}^{m \times n}, W \in \mathbb{R}^{m \times m}, Y \in \mathbb{R}^{n \times m}$ and IQC multiplier $\Lambda \in \mathbb{D}_+^m$ with m, n as the dimensions of hidden unit and input, respectively. The aim of this section is to construct a parameterization such that the large-scale SDP constraint (5) holds, i.e., $Y = U^\top \Lambda$ and

$$H = 2\Lambda - W^\top \Lambda - \Lambda W = \begin{bmatrix} 2\Lambda_1 & -W_2^\top \Lambda_2 & & \\ -\Lambda_2 W_2 & 2\Lambda_2 & -W_3^\top \Lambda_3 & \\ & \ddots & \ddots & \ddots \\ & & -\Lambda_{L-1} W_{L-1} & 2\Lambda_{L-1} & -W_L^\top \Lambda_L \\ & & & -\Lambda_L W_L & 2\Lambda_L \end{bmatrix} \geq \frac{2}{\gamma} Y^\top Y \quad (18)$$

Since $H \succeq 0$ has band structure, it can be represented by $H = XX^\top$ Davis (2006). Moreover, from Lemma 3 of Rantzer (1996) we have that any U, Y satisfying $Y = U^\top \Lambda$ and $XX^\top \succeq 2/\gamma Y^\top Y$ can be represented by

$$U = \sqrt{\gamma/2} \Lambda^{-1} X Q, \quad Y = \sqrt{\gamma/2} Q^\top X^\top \quad (19)$$

where $Q \in \mathbb{R}^{m \times n}$ with $QQ^\top \preceq I$. The remaining task is to find X such that $H = XX^\top$ has the same sparse structure as (18), which was solved by Wang and Manchester (2023). For self-contained purpose, we provide detail construction as follows. First, we further parameterize $X = \Psi P$, where $\Psi = \text{diag}(\Psi_1, \dots, \Psi_L)$ with $\Psi_k \in \mathbb{D}_+^{m_k}$ and

$$P = \begin{bmatrix} A_1 & & & \\ -B_2 & A_2 & & \\ & \ddots & \ddots & \\ & & -B_L & A_L \end{bmatrix}.$$

By comparing $H = \Psi P P^\top \Psi$ with (18) we have

$$H_{kk} = \Psi_k (B_k B_k^\top + A_k A_k^\top) \Psi_k = 2\Lambda_k, \quad H_{k-1,k} = -\Psi_k B_k A_{k-1}^\top = -\Lambda_k W_k,$$

which further leads to

$$\Psi_k^2 = 2\Lambda_k, \quad B_k B_k^\top + A_k A_k^\top = I, \quad W_k = 2\Psi_k^{-1} B_k A_{k-1}^\top \Psi_{k-1} \quad k = 1, \dots, L, \quad (20)$$

with $B_1 = 0$. We have converted the large-scale SDP constraint (18) into many simple and small-scale constraints such as

$$\Psi_k^2 = 2\Lambda_k, \quad R_k R_k^\top = I, \quad QQ^\top \preceq I \quad (21)$$

with $R_k = [B_k \ A_k]$, which further can be easily parameterized via the Cayley transformation (6), see Section 3.3. From Proposition 3.5 we have that the transformation between (18) and (21) is equivalent.

An equivalent model representation. The model weight parameter U, Y, W defined in (7) can be rewritten as $U = \sqrt{2\gamma} \Psi^{-1} S$, $Y = \sqrt{\gamma/2} S^\top \Psi^{-1}$ and $W = \Psi^{-1} W \Psi$ with

$$S = \begin{bmatrix} S_1 \\ S_2 \\ \vdots \\ S_L \end{bmatrix} = \begin{bmatrix} A_1 Q_1 \\ A_2 Q_2 - B_2 Q_1 \\ \vdots \\ A_L Q_L - B_L Q_{L-1} \end{bmatrix}, \quad V = \begin{bmatrix} 0 & & & \\ V_2 & 0 & & \\ & \ddots & \ddots & \\ & & V_L & 0 \end{bmatrix} = \begin{bmatrix} 0 & & & \\ 2B_2 A_1^\top & 0 & & \\ & \ddots & \ddots & \\ & & 2B_L A_{L-1}^\top & 0 \end{bmatrix} \quad (22)$$

where $Q = [Q_1^\top \ \cdots \ Q_L^\top]^\top$. Then, the network (4) can be written as

$$z = \sigma(\Psi^{-1} V \Psi z + \sqrt{2\gamma} \Psi^{-1} S x + b), \quad y = \mu x + \sqrt{\gamma/2} S^\top \Psi z. \quad (23)$$

By introducing the new hidden state $\hat{z} = \Psi z$ and bias $\hat{b} = \Psi b$, we obtain an equivalent form:

$$\hat{z} = \hat{\sigma}(V\hat{z} + \sqrt{2\gamma}Sx + \hat{b}), \quad y = \mu x + \sqrt{\gamma/2}S^\top \hat{z} + b_y. \quad (24)$$

This representation is useful for model inverse via monotone operator splitting, see the next section. We now give a lemma which will be used later for proving some propositions.

Lemma A.1. *For the matrices V, S defined in (22) we have*

$$2I - V - V^\top \succeq 0, \quad 2I - SS^\top \succeq 0. \quad (25)$$

Proof. First, we have

$$2I - (V + V^\top) = 2 \begin{bmatrix} I & -A_1 B_2^\top & & \\ -B_2 A_1^\top & I & -A_2 B_3^\top & \\ & -B_3^\top A_2 & \ddots & \ddots \\ & & \ddots & \ddots \end{bmatrix} \succeq 0 \quad (26)$$

where the inequality is obtained by sequentially applying the fact $A_k A_k^\top + B_k B_k^\top = I$ and Schur complement to the top diagonal block. For the inequality on S , we have

$$\begin{aligned} 2I - SS^\top &= 2I - PQQ^\top P^\top \succeq 2I - PP^\top \\ &= 2I - \begin{bmatrix} A_1 & & & \\ -B_2 & A_2 & & \\ & \ddots & \ddots & \\ & & -B_L & A_L \end{bmatrix} \begin{bmatrix} A_1 & & & \\ -B_2 & A_2 & & \\ & \ddots & \ddots & \\ & & -B_L & A_L \end{bmatrix}^\top = \begin{bmatrix} I & A_1 B_2^\top & & \\ B_2 A_1^\top & I & A_2 B_3^\top & \\ & B_3^\top A_2 & \ddots & \ddots \\ & & \ddots & \ddots \end{bmatrix} \succeq 0. \end{aligned}$$

Similarly, the last inequality can be established by sequentially applying the Schur complement to the top diagonal block. \square

B Monotone Operator Splitting for Computing Model Inverse

Inspired by Winston and Kolter (2020); Revay et al. (2020), we try to compute $x = \mathcal{F}^{-1}(y)$ via operator splitting method. We first present some background of monotone operator theory based on the survey Ryu and Boyd (2016), and then reformulate the model inverse as a three-operator splitting problem.

B.1 Monotone operator

An *operator* is a set-valued or single-valued map defined by a subset of the space $\mathcal{A} \subseteq \mathbb{R}^n \times \mathbb{R}^n$; we use the notation $\mathcal{A}(x) = \{y \mid (x, y) \in \mathcal{A}\}$. For example, the affine operator is defined by $\mathcal{L}(x) = \{(x, Wx + b) \mid x \in \mathbb{R}^n\}$. Another important example is the subdifferential operator $\partial f = \{(x, \partial f(x))\}$ for a proper function $f : \mathbb{R}^n \rightarrow \mathbb{R} \cup \{\infty\}$ with $f(z) = \infty$ for $z \notin \text{dom } f$, where $\partial f(x) = \{g \in \mathbb{R}^n \mid f(y) \geq f(x) + \langle y - x, g \rangle, \forall y \in \mathbb{R}^n\}$. An operator \mathcal{A} has a Lipschitz bound of L if $\|u - v\| \leq L\|x - y\|$ for all $(x, u), (y, v) \in \mathcal{A}$. It is *non-expansive* if $L = 1$ and *contractive* if $L < 1$. \mathcal{A} is *strongly monotone* with $m > 0$ if

$$\langle u - v, x - y \rangle \geq m\|x - y\|, \quad \forall (x, u), (y, v) \in \mathcal{A}. \quad (27)$$

If the above inequality holds for $m = 0$, we call \mathcal{A} a monotone operator. Similarly, \mathcal{A} is said to be *inverse monotone* with ρ if $\langle u - v, x - y \rangle \geq \rho\|u - v\|$, $\forall (x, u), (y, v) \in \mathcal{A}$. An operator is called *maximal monotone* if no other monotone operator strictly contains it. The linear operator \mathcal{L} is m -strongly monotone if $W + W^\top \succeq 2mI$, and ρ -inverse monotone if $W + W^\top \succeq 2\rho W^\top W$. A subdifferential ∂f is maximal monotone if and only if f is a convex closed proper (CCP) function. Here are some basic operations for operators:

Table 1: A list of common activation functions and their associated convex proper $f(z)$ whose proximal operator is $\sigma(x)$ Revay et al. (2020). For $z \notin \text{dom } f$, we have $f(z) = \infty$. In the case of Softplus activation, $\text{Li}_s(z)$ is the polylogarithm function.

Activation	$\sigma(x)$	Convex $f(z)$	$\text{dom } f$
ReLU	$\max(x, 0)$	0	$[0, \infty)$
LeakyReLU	$\max(x, 0.01x)$	$\frac{99}{2} \min(z, 0)^2$	\mathbb{R}
Tanh	$\tanh(x)$	$\frac{1}{2} \left[\ln(1 - z^2) + z \ln \left(\frac{1+z}{1-z} \right) - z^2 \right]$	$(-1, 1)$
Sigmoid	$1/(1 + e^{-x})$	$z \ln z + (1 - z) \ln(1 - z) - \frac{z^2}{2}$	$(0, 1)$
Arctan	$\arctan(x)$	$-\ln(\cos z) - \frac{z^2}{2}$	$(-1, 1)$
Softplus	$\ln(1 + e^x)$	$-\text{Li}_2(e^z) - i\pi z - z^2/2$	$(0, \infty)$

- the operator sum $\mathcal{A} + \mathcal{B} = \{(x, y + z) \mid (x, y) \in \mathcal{A}, (x, z) \in \mathcal{B}\}$;
- the composition $\mathcal{A}\mathcal{B} = \{(x, z) \mid \exists y \text{ s.t. } (x, y) \in \mathcal{A}, (y, z) \in \mathcal{B}\}$;
- the inverse operator $\mathcal{A}^{-1} = \{(y, x) \mid (x, y) \in \mathcal{A}\}$;
- the *resolvent* operator $R_{\mathcal{A}} = (I + \alpha\mathcal{A})^{-1}$ with $\alpha > 0$;
- the *Cayley* operator $C_{\mathcal{A}} = 2R_{\mathcal{A}} - I$.

Note that the resolvent and Cayley operators are non-expansive for any maximal monotone \mathcal{A} , and are contractive if \mathcal{A} is strongly monotone. For a linear operator \mathcal{L} we have $R_{\mathcal{L}}(x) = (I + \alpha W)^{-1}(x - ab)$. For a subdifferential operator ∂f , its resolvent is $R_{\partial f}(x) = \text{prox}_f^\alpha(x) := \arg \min_z 1/2\|x - z\| + \alpha f(z)$, which is also called the *proximal operator*.

Activation as proximal operator. As shown in Li et al. (2019); Revay et al. (2020), many popular slope-restricted scalar activation functions can also be treated as proximal operators. To be specific, if $\sigma : \mathbb{R} \rightarrow \mathbb{R}$ is slope-restricted in $[0, 1]$, then there exists a convex proper function f such that $\sigma(\cdot) = \text{prox}_f^1(\cdot)$. For self-contained purpose, we provide a list of common activations and their associated convex proper functions in Table 1, which can also be found in Revay et al. (2020); Li et al. (2019).

B.2 Operator splitting

Many optimization problems (e.g. convex optimization) can be formulated as one of finding a zero of an appropriate monotone operator \mathcal{F} , i.e., find $x \in \mathbb{R}^n$ such that $0 \in \mathcal{F}(x)$. Note that x is a solution if and only if it is a fixed point $x = \mathcal{T}(x)$ with $\mathcal{T} = I - \alpha\mathcal{F}$ for any nonzero $\alpha \in \mathbb{R}$. The corresponding fixed point iteration is $x^{k+1} = \mathcal{T}(x^k) = x^k - \alpha\mathcal{F}(x^k)$. If \mathcal{F} is m -strongly monotone and L -Lipschitz, then this iteration converges by choosing $\alpha \in (0, 2m/L^2)$. The optimal convergence rate is $1 - (m/L)^2$, given by $\alpha = m/L^2$.

If \mathcal{F} contains some non-smooth components, we then split \mathcal{F} into two or three maximal operators:

$$\text{two-operator splitting problem: } 0 \in \mathcal{A}(x) + \mathcal{B}(x) \quad (28)$$

$$\text{three-operator splitting problem: } 0 \in \mathcal{A}(x) + \mathcal{B}(x) + \mathcal{C}(x) \quad (29)$$

where \mathcal{A} , \mathcal{B} , and \mathcal{C} are maximal monotone. The main benefit of such splitting is that the resolvent or Cayley operators for individual operator are easy to evaluate, which further leads to more computationally efficient algorithms. For two-operator splitting problem, some popular algorithms include

- forward-backward splitting (FBS) $x = R_{\mathcal{B}}(I - \alpha\mathcal{A})(x)$
- forward-backward-forward splitting (FBFS) $x = ((I - \alpha\mathcal{A})R_{\mathcal{B}}(I - \alpha\mathcal{A}) + \alpha\mathcal{A})(x)$
- Peaceman-Rachford splitting (PRS) $z = C_{\mathcal{A}}C_{\mathcal{B}}(z)$, $x = R_{\mathcal{B}}(z)$
- Douglas-Rachford splitting (DRS) $z = (1/2I + 1/2C_{\mathcal{A}}C_{\mathcal{B}})(z)$, $x = R_{\mathcal{B}}(z)$

where the corresponding fixed-point iterations, the choices of hyper-parameter α and convergence results can be found in Ryu and Boyd (2016). For three-operator splitting problem, the Davis-Yin splitting (DYS) Davis and Yin (2017) can be expressed by $z = \mathcal{T}(z)$, $x = R_{\mathcal{B}}(z)$ where $\mathcal{T} = C_{\mathcal{A}}(C_{\mathcal{B}} - \alpha\mathcal{C}R_{\mathcal{B}}) - \alpha\mathcal{C}R_{\mathcal{B}}$.

B.3 Operator splitting perspective for \mathcal{F}^{-1}

As shown in the proof of Proposition 4.2, By applying the forward-backward splitting with parameter $\alpha = 1$, we can compute the solution z via the following iteration:

$$z^{k+1} = R_{\mathcal{B}}(z^k - \widehat{\mathcal{A}}(z^k)) = \dot{\sigma}((V - \gamma/\mu SS^\top)z^k + b_z).$$

It is worth pointing out that the above iteration may not converge for the choice of $\alpha = 1$. In practice we often use more stable and faster two-operator splitting algorithms (e.g., PRS or DRS), see Winston and Kolter (2020); Revay et al. (2020). In this work, the motivation for further decomposing the monotone operator $\widehat{\mathcal{A}}$ into two monotone operators \mathcal{A}, \mathcal{C} is that $R_{\mathcal{A}}$ is a large-scale linear equation with nice sparse structure while $R_{\widehat{\mathcal{A}}}$ is dense due to the full weight matrix in \mathcal{C} .

Fixed-point iteration. We now apply the DYS algorithm from Davis and Yin (2017) to $0 \in \mathcal{A}(z) + \mathcal{B}(z) + \mathcal{C}(z)$, resulting in the following fixed-point iteration:

$$\begin{aligned} z^{k+1/2} &= R_{\mathcal{B}}(u^k) = \mathbf{prox}_f^\alpha(u^k) \\ u^{k+1/2} &= 2z^{k+1/2} - u^k \\ z^{k+1} &= R_{\mathcal{A}}(u^{k+1/2} - \alpha\mathcal{C}(z^{k+1/2})) \\ u^{k+1} &= u^k + z^{k+1} - z^{k+1/2} \end{aligned} \quad (30)$$

where the third line is a large-scale sparse linear equation of the form

$$\begin{bmatrix} (1+\alpha)I & & & \\ -\alpha V_{21} & (1+\alpha)I & & \\ \ddots & \ddots & \ddots & \\ & -\alpha V_{L,L-1} & (1+\alpha)I & \end{bmatrix} \begin{bmatrix} z_1^{k+1} \\ z_2^{k+1} \\ \vdots \\ z_L^{k+1} \end{bmatrix} = u^{k+1/2} + \alpha \left(b_z - \frac{\gamma}{\mu} SS^\top z^{k+1/2} \right).$$

By introducing $v^{k+1/2} = b_z - \gamma/\mu SS^\top z^{k+1/2}$, we have

$$z_0^{k+1} = 0, \quad z_l^{k+1} = \frac{\alpha}{1+\alpha} (V_{l,l-1} z_{l-1}^{k+1} + v_l^{k+1/2}) + \frac{1}{1+\alpha} u_l^{k+1/2}, \quad l = 1, \dots, L. \quad (31)$$

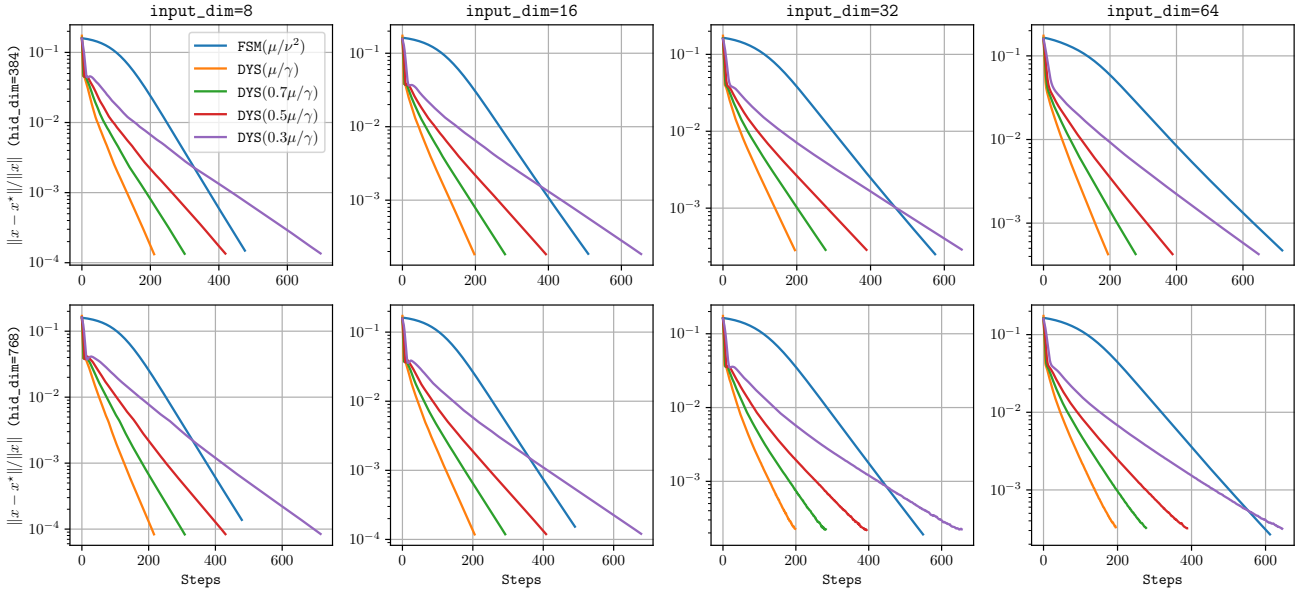


Figure 9: Forward step method (FSM) vs Davis-Yin splitting (DYS) applied to randomly initialized μ -monotone and ν -Lipschitz layer with different input and hidden unit dimensions. We observe that DYS converges faster for larger α . If α is close to the bound μ/γ with $\gamma = \nu - \mu$, it has a much faster rate than FSM.

Convergence range for the hyper-parameter α . From the previous paragraph, we know that (14) is equivalent to the FPI (30). From Theorem 1.1 of Davis and Yin (2017), we have that (30) converges for any $\alpha \in (0, 2\beta)$ with β as the inverse-monotone bound of \mathcal{C} . From Lemma A.1 we have $2I \succeq S^\top S$ and

$$\frac{2\gamma}{\mu} SS^\top \succeq \frac{\gamma}{\mu} S(S^\top S)S^\top = \frac{\mu}{\gamma} (\gamma/\mu SS^\top)^2 = 2\beta(\gamma/\mu SS^\top)^2$$

i.e., $\mathcal{C}(z)$ is inverse monotone with $\beta = \mu/(2\gamma)$. Therefore, (14) converges for any $\alpha \in (0, \mu/\gamma)$. Since $\gamma = \nu - \mu$ and $\tau = \nu/\mu$, we then obtain the convergence range in term of model distortion τ , i.e., $\alpha \in (0, 1/(\tau - 1))$. Larger α often implies faster convergence rate, see Figure 9.

C Proofs

C.1 Proof of Theorem 3.2

We consider the neural network $\mathcal{H} : x \rightarrow \tilde{y}$ defined by

$$v = Wz + Ux + b, \quad z = \sigma(v), \quad \tilde{y} = Yz + b_y. \quad (32)$$

Since $\mathcal{F}(x) = \mu x + \mathcal{H}(x)$, then \mathcal{F} is μ -strongly monotone and ν -Lipschitz if \mathcal{H} is monotone and γ -Lipschitz with $\gamma = \nu - \mu$.

For any pair of solutions $s_1 = (x_1, v_1, z_1, \tilde{y}_1)$ and $s_2 = (x_2, v_2, z_2, \tilde{y}_2)$, their difference $\Delta s = s_1 - s_2$ satisfies

$$\Delta v = W\Delta z + U\Delta x, \quad \Delta z = J_\sigma(v_1, v_2)\Delta v, \quad \Delta \tilde{y} = Y\Delta z \quad (33)$$

where J_σ is a diagonal matrix with $[J_\sigma]_{ii} \in [0, 1]$ since σ is an elementwise activation with slope restricted in $[0, 1]$. For any $\Lambda \in \mathbb{D}_+^m$ we have

$$\langle \Delta v - \Delta z, \Lambda \Delta z \rangle = \Delta v^\top (I - J_\sigma) \Lambda J_\sigma \Delta v \geq 0, \quad \forall \Delta v \in \mathbb{R}^m. \quad (34)$$

Based on (33), (34) and Condition (5) we have

$$\begin{aligned}
& \langle \Delta x, \Delta \tilde{y} \rangle - \langle \Delta v - \Delta z, \Lambda \Delta z \rangle \\
&= \langle \Delta x, Y \Delta z \rangle - \langle (W - I) \Delta z + U \Delta x, \Lambda \Delta z \rangle \\
&= \langle \Delta x, Y \Delta z \rangle - \langle \Delta x, U^\top \Lambda \Delta z \rangle + \langle (I - W) \Delta z, \Lambda \Delta z \rangle \\
&= \mathbf{1}/2 \Delta z^\top (\Lambda(I - W) + (I - W^\top) \Lambda) \Delta z \geq \|Y \Delta z\|^2 \geq 0,
\end{aligned} \tag{35}$$

which further implies $\langle \Delta x, \Delta y \rangle - \mu \|\Delta x\|^2 \geq \langle \Delta v - \Delta z, \Lambda \Delta z \rangle \geq 0$. Thus, \mathcal{H} is monotone. We can use the similar technique to derive the Lipschitz bound of \mathcal{H} . Firstly we have

$$\begin{aligned}
& \gamma \|\Delta x\|^2 - \frac{1}{\gamma} \|\Delta \tilde{y}\|^2 - 2 \langle \Delta v - \Delta z, \Lambda \Delta z \rangle \\
&= \gamma \|\Delta x\|^2 - \frac{1}{\gamma} \|\Delta \tilde{y}\|^2 + 2 \langle (I - W) \Delta z, \Lambda \Delta z \rangle - 2 \langle U \Delta x, \Lambda \Delta z \rangle \\
&= \gamma \|\Delta x\|^2 - 2 \langle \Delta x, \Delta \tilde{y} \rangle - \frac{1}{\gamma} \|\Delta \tilde{y}\|^2 + \Delta z^\top (2\Lambda - \Lambda W - W^\top \Lambda) \Delta z \\
&\geq \gamma \|\Delta x\|^2 - 2 \langle \Delta x, \Delta \tilde{y} \rangle - \frac{1}{\gamma} \|\Delta \tilde{y}\|^2 + \frac{2}{\gamma} \|Y \Delta z\|^2 = \left\| \sqrt{\gamma} \Delta x - \frac{1}{\sqrt{\gamma}} \Delta \tilde{y} \right\|^2 \geq 0.
\end{aligned} \tag{36}$$

Due to (34) we can further obtain $\gamma^2 \|\Delta x\|^2 \geq \|\Delta \tilde{y}\|^2$, i.e., \mathcal{H} is γ -Lipschitz.

C.2 Proof of Proposition 3.5

Sufficient part: (7) \Rightarrow (5). From (19) we have that $Y = U^\top \Lambda$. We check the inequality part of (5) as follows:

$$2\Lambda - W^\top \Lambda - \Lambda W = \Psi P P^\top \Psi = X X^\top \succeq X Q Q^\top X^\top = \frac{2}{\gamma} Y^\top Y.$$

Necessary part: (5) \Rightarrow (7). Since $H \succeq 0$ has band structure, then it can be decomposed into $H = X X^\top$ where X has the following block lower triangular structure Davis (2006):

$$X = \begin{bmatrix} X_{11} & & & \\ X_{21} & X_{22} & & \\ & \ddots & \ddots & \\ & & X_{L,L-1} & X_{LL} \end{bmatrix}.$$

For this special case, a way to construct X from Λ, W and further computation of the free parameters $d, F_k^a, F_k^b, F^q, F^*$ can be found in Wang and Manchester (2023). Finally, we need to show that $X X^\top \succeq 2/\gamma Y^\top Y$ is equivalent to $Y = \sqrt{\gamma/2} Q^\top X^\top$ for some $Q Q^\top \preceq I$, which can be directly followed by Lemma 3 of Rantzer (1996).

C.3 Proof of Proposition 4.1

From Lemma A.1 we have

$$2I - (V - \gamma/\mu S S^\top) - (V - \gamma/\mu S S^\top)^\top = 2I - V - V^\top + 2\gamma/\mu S S^\top \succeq 2\gamma/\mu S S^\top \succeq 0. \tag{37}$$

Then, the equilibrium network (12) is well-posed by Theorem 1 of Revay et al. (2020).

C.4 Proof of Proposition 4.2

We first show that $0 \in \mathcal{A}(z) + \mathcal{B}(z) + \mathcal{C}(z)$ is a monotone operator splitting problem. It is obvious that \mathcal{B}, \mathcal{C} are maximal monotone operators. From Lemma A.1 we have $(I - V) + (I - V)^\top \succeq 0$, i.e. \mathcal{A} is also monotone. Then, we show that the above operator splitting problem shares the same set of equilibrium points with the model inverse (12). First, we rewrite it into a two-operator splitting problem $0 \in \widehat{\mathcal{A}}(z) + \mathcal{B}(z)$ where $\widehat{\mathcal{A}} = \mathcal{A} + \mathcal{C}$. By applying the forward-backward splitting with parameter $\alpha = 1$, we can compute the solution z via the following iteration:

$$z^{k+1} = R_{\mathcal{B}}(z^k - \widehat{\mathcal{A}}(z^k)) = \mathbf{prox}_f^1(z^k - (I - V + \gamma/\mu S S^\top) z^k + b_z) = \hat{\sigma}((V - \gamma/\mu S S^\top) z^k + b_z).$$

Thus, any solution z^* of the equilibrium network (12) is also an equilibrium point of the above iteration.

C.5 Proof of Proposition 5.1

First, we have $\nabla f(x) = G^\top(x)\mathcal{G}(x)$ where $G(x) = \nabla \mathcal{G}(x)$ satisfies $\|G(x)\| \geq \mu$. Then, the PL inequality holds for f with $m = \mu^2$, i.e.,

$$\frac{1}{2}\|\nabla f(x)\|^2 = \frac{1}{2}\mathcal{G}(x)^\top G(x)^\top G(x)\mathcal{G}(x) \geq \frac{\mu^2}{2}\|\mathcal{G}(x)\|^2 = \mu^2(f(x) - f^*). \quad (38)$$

D Experiments

D.1 Training details

For all experiments, we choose ReLU as our default activation and use Adam Kingma and Ba (2015) with one-cycle linear learning rate Coleman et al. (2017) except the NGP case which use a fixed rate. For the NGP case, we use the cross entropy loss while the L2 loss is used for the rest of the examples. For our proposed BiLipNet, we fixed the free parameter $F_* = 0$, which implies that $Q^\top Q = I$ instead of $Q^\top Q \preceq I$. By enforcing all singular values of Q to be 1 (as suggested by Prach and Lampert (2022)), this can improve the model training when there are multiple monotone and Lipschitz layers. Dataset and model architectures are described as follows.

1D Step function. The target function is a step function

$$f(x) = \begin{cases} 2, & x > 0 \\ -2, & x < 0 \end{cases}$$

which is monotone and 0-Lipschitz everywhere except the singularity point $x = 0$. We try to fit this curve with $(0.1, 10)$ -Lipschitz models. The optimal fit is a linear piecewise continuous function with slope of 10 near $x = 0$ and slope of 0.1 near $x = \pm 2$. We take 1000 random samples from $[-2, 2]$ for training. Our model (BiLipNet) is an one-layer residual network $\mathcal{F}(x) = \mu x + \mathcal{H}(x)$ where \mathcal{H} has 8 hidden layers of width 32, giving the model 15.8K parameters. We compare to i-ResNet Chen et al. (2019) and i-DenseNet Perugachi-Diaz et al. (2021), where the nonlinear block \mathcal{H} has 2 and 4 hidden layers, respectively. For those two models, we test for depth from 2 to 8 with proper hidden width (so that they has similar amount of parameters). And the empirical Lipschitz bound is computed via finite difference over the test data. As shown in Figure 1, our model achieves much tighter bounds than other models.

Neural Gaussian process. We take 1000 two-moon data points as training data and 1000 Gaussian samples with mean $(1.3, -1.8)$ and variance $(0.02, 0.01)$ as OOD data. For all models, we use fixed input weight to mapping the 2D input into 128D hidden space, then perform hidden space transformation using bi-Lipschitz models, and

finally add a Gaussian process as the output layer. SNGP uses 3 residual layer $x + \mathcal{H}(x)$ where the Lipschitz bound of \mathcal{H} is $c < 1$. BiLipNet has one monotone and Lipschitz layer with two orthogonal layer, i.e., $K = 1$ for (10). The nonlinear block \mathcal{H} of our model has 6 hidden layers with width of 32. Both models are chosen to have the same amount of parameters, roughly $233K$.

2D Rosenbrock function. The true function is a Rosenbrock function defined by

$$r(x, y) = \frac{1}{200}(x - 1)^2 + \frac{1}{2}(y - x^2)^2.$$

Note that we use a scaling factor of 1/200 for the classic Rosenbrock function. The above function is non-convex but has one minimum at $(1, 1)$. We also consider the combination of the above Rosenbrock function with the following 2D Sine function:

$$s(x, y) = 0.25(\sin(8(x - 1) - \pi/2) + \sin(8(y - 1) - \pi/2) + 2).$$

In this case $r(x, y) + s(x, y)$ still has a unique global minimum at $(1, 1)$. But there are many local minima. We take 5K random training samples from the domain $[-2, -2] \times [-1, 3]$. The proposed BiLipNet contains two monotone and Lipschitz layers (i.e., $K = 2$ for (10)). The nonlinear block \mathcal{H} has 4 hidden layers of width 128. The model size is roughly 16K. The ICNN model has 8 hidden layers with width of 180. The MLP has hidden units of $[128, 256, 256, 512]$. We trained i-ResNet and i-DenseNet with different depth and width such that the total amount of parameters is comparable with BiLipNet.

Parametric Rosenbrock function. We consider the following parametric Rosenbrock function

$$r(x, y; p) = \frac{1}{200}(x - a)^2 + \frac{1}{2}(y - bx^2)^2, \quad p = (a, b) \in [-1, 1]^2.$$

We take 10K random training data. The partially BiLipNet contains 3 orthogonal layers, and 2 monotone and Lipschitz layers (the \mathcal{H} block of each layer has 4 hidden layer with width 128). The bias term of each orthogonal layer is produced by an MLP with hidden units of $[64, 128, 2]$ while the bias for those hidden units inside the \mathcal{H} block is generated by an MLP of $[64, 128, 256, 512]$. The model's bi-Lipschitz bound is chosen to be $(0.04, 16)$. The resulting model size is 604K.

ND Rosenbrock function. We also consider the N -dimensional (with $N = 20$) Rosenbrock function:

$$R_N(x) = \frac{1}{N-1} \sum_{i=1}^{N-1} r(x_i, x_{i+1})$$

which is non-convex and has a unique global minimum at $(1, 1, \dots, 1)$. Besides it also has many local minima. We take 10K random samples over the domain $[-2, 2]^{20}$ and do training with batch size of 200. Note that the data size is very small compared to the dimension. We then use 500K samples for testing. BiLipNet has two monotone and Lipschitz layers (i.e., $K = 2$ for (10)) where each layer has a nonlinear block \mathcal{H} with 8 hidden layer of width 256 (model size $\sim 2.1M$). For the i-ResNet/i-DenseNet, we try different depths from 2 to 10 and observe that depth of 5 yields slightly better results. The width of hidden layer is chosen so that it has a similar amount of parameters as BiLipNet.

D.2 Extra results

Some extra results for uncertainty quantification via neural Gaussian process and surrogate loss learning are shown in Figure 10 and Figure 11, respectively.

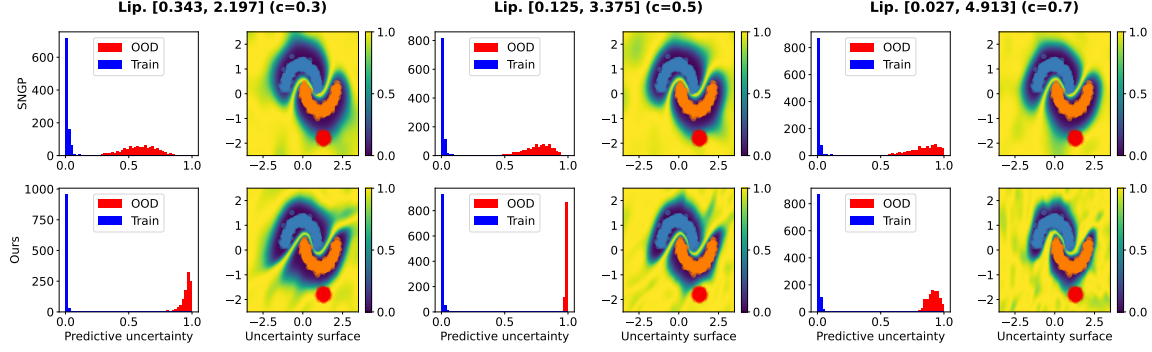


Figure 10: Uncertainty qualification via neural Gaussian process with different bi-Lipschitz bound specifications on the hidden space mapping.

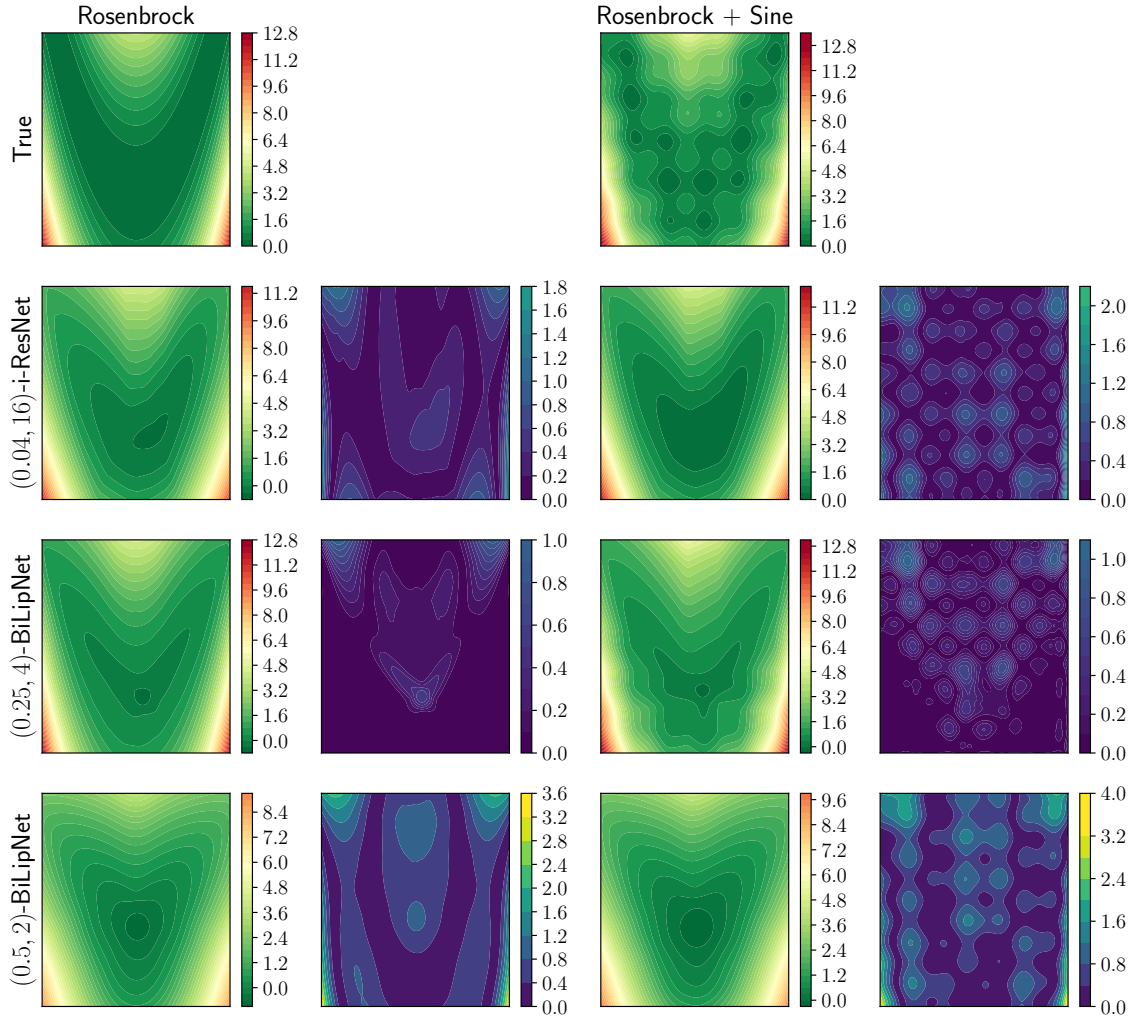


Figure 11: Additional results for Learning a surrogate loss for the Rosenbrock and Rosenbrock + Sine functions. The first row contains the true functions while the remaining rows show learned functions and errors for various surrogate loss models. Our model has the flexibility of capturing the non-convex sub-level sets, but can also fit smoothed representations by reducing the distortion parameter.